JOURNAL OF GUIDANCE, CONTROL, AND DYNAMICS
Vol. 17, No. 5, September–October 1994

Hybrid Approach to Near-Optimal Launch Vehicle Guidance

Martin S. K. Leung* and Anthony J. Calise†
Georgia Institute of Technology, Atlanta, Georgia 30332

This paper evaluates a proposed hybrid analytic/numerical approach to launch vehicle guidance for ascent to orbit injection. The feedback guidance approach is based on a piecewise nearly analytic solution evaluated using a collocation method. Each piece of the solution obeys a bilinear tangent law for the thrust-vector angle, which serves as an intelligent interpolating function for the collocation method. The zero-order solution is then improved through a regular perturbation analysis, wherein the neglected dynamics are accounted for in the first-order term. For real-time implementation, the guidance approach requires solving a set of small dimension nonlinear algebraic equations and performing quadrature. Assessment of performance and reliability are carried out through closed-loop simulation for a vertically launched two-stage heavy-lift capacity vehicle to a low-Earth transfer orbit. The solutions are compared with optimal solutions generated from a multiple shooting code. In the example the guidance approach delivers near-optimal performance and accurately satisfies the terminal constraints. The control computation is completed in tenths of a second on a SPARCstation 1. Wind shear effects and control constraints are also addressed.

Introduction

TRADITIONAL launch vehicle guidance may involve either two or three different phases.[1–3] The first is an open-loop guidance phase for the atmospheric portion of flight, which typically flies with a nonoptimal piecewise linear attitude control program. The second is a closed-loop guidance phase for the exoatmospheric portion of flight.[1,2] This has an analytic solution under certain assumptions. Then a third closed-loop phase may be required when the vehicle is approaching orbital conditions for final precision orbit injection.[1] Though the guidance approaches for the exoatmospheric phases are efficient and reliable, the use of open-loop guidance for the atmospheric flight phase has been a cause of costly launch delays. This occurs when the actual wind profile differs significantly from the mean profile used in computing the attitude control program. The desire to reduce or eliminate this source of launch delay has led to a renewed interest in developing a closed-loop guidance approach for the atmospheric flight phase.

Numerical approaches to optimal guidance typically employ either nonlinear programming[4–6] or multiple shooting.[7] To be useful as a feedback guidance solution, it is essential that these approaches converge quickly and reliably at each instant when the solution is updated during the flight. At the other end of the spectrum lie analytic approaches that attempt to correct the exoatmospheric guidance solution by a regular perturbation approach.[8,9] The viewpoint taken here is that the atmospheric effects (in addition to spherical and rotating Earth effects) act as perturbations from a zero-order model whose solution obeys the well-known bilinear tangent guidance law. A quadrature is required to correct the zero-order solution for these perturbing effects. Unfortunately, numerical experience with this approach has revealed that the atmospheric effects are too large to be neglected in the zero-order solution.[10]

In this paper we combine the numerical method of collocation[6,11,16] with the regular perturbation approach developed in Ref. 8. The objective is to account for the atmospheric effects in the zero-order solution. When compared with the use of collocation alone, the hybrid approach greatly reduces the number of simultaneous algebraic equations that have to be solved at each control update and therefore should be more suitable for real-time applications than a purely numerical approach. A second advantage is that the bilinear tangent law is preserved, and therefore a single form of guidance is employed over the entire trajectory. A first-order correction is computed to correct the solution for spherical Earth effects. Although not considered in this paper, the analysis can readily be extended to include rotating Earth effects as well.

We begin with a brief outline of the hybrid approach, which has been detailed and illustrated by simple examples in Ref. 12. Next we illustrate how the hybrid approach applies to the launch vehicle ascent trajectory guidance problem, including first-order correction for neglected dynamics. Finally, numerical results are presented that evaluate the efficiency and accuracy of the hybrid approach.

Summary of the Hybrid Approach

This section summarizes the main results from Ref. 12, which presents a detailed explanation on how to combine the methods of regular perturbation analysis and collocation for numerical solution of optimal control problems.

Regular Perturbation Analysis

The optimal control problem formulation considered here is to maximize a performance index that is a function of the terminal states and time, subject to nonlinear dynamic constraints:

$$J = \max_u \{\phi(x,t)\}|_{t_f} \tag{1}$$

$$\dot{x} = f(x,u,t) + \varepsilon g(x,u,t); \qquad x(t_0) = x_0, \quad t \in [t_0, t_f] \tag{2}$$

and the terminal time constraints $\psi_i[x(t_f)] = 0, i = 1, \ldots, p \leq n$. In Eq. (2), x is an n-dimensional state vector, u is an m-dimensional control vector, and ε is an expansion parameter. The final time is open. Hence, the necessary conditions for optimality are

$$\dot{\lambda} = -H_x; \qquad \lambda(t_f) = \Phi_x\big|_{t_f} \tag{3}$$

$$H_u = \lambda^T(f_u + \varepsilon g_u) = 0 \tag{4}$$

$$H = \lambda^T(f + \varepsilon g); \qquad H(t_f) = -\Phi_t\big|_{t_f}, \quad \Phi = \phi + \nu^T\psi \tag{5}$$

In a regular perturbation analysis, the objective is to approximate the solution to Eqs. (2–5) by an asymptotic series of the form $(\bullet) = (\bullet)_0 + (\bullet)_1\varepsilon + (\bullet)_2\varepsilon^2 + \ldots$, where $(\bullet)$ denotes all of the variables (x, λ, u, ν, and $T = t_f - t_0$) that depend on ε.

Received May 21, 1992; revision received Sept. 27, 1993; accepted for publication Oct. 4, 1993.

*Currently Project Manager, Business Development, Champion Technology Ltd., 9/F Kantone Centre, 1 Ning Foo Street, Chai Wan, Hong Kong. Member AIAA.

†Professor, School of Aerospace Engineering. Fellow AIAA.

Zero-Order Problem

It is shown in Ref. 12 that the necessary conditions for the zero-order problem can be expressed as

$$\frac{\partial x_0}{\partial \hat{t}} = \frac{\partial H_0}{\partial \lambda_0}; \qquad x_0(t_0) = x_0; \qquad \psi[x_0(t_0 + T_0)] = 0 \tag{6}$$

$$\frac{\partial \lambda_0}{\partial \hat{t}} = -\frac{\partial H_0}{\partial x_0}; \quad \lambda_0(\hat{t} = t_0 + T_0) = \left.\frac{\partial \Phi(x_0, \hat{t})}{\partial x_0}\right|_{\hat{t}=t_0+T_0} \tag{7}$$

$$\frac{\partial H_0}{\partial u_0} = 0 \tag{8}$$

$$H_0 = \lambda_0^T f(x_0, u_0, \hat{t})$$

$$H_0(\hat{t} = t_0 + T_0) = -\left.\frac{\partial \Phi(x_0, \hat{t})}{\partial \hat{t}}\right|_{\hat{t}=t_0+T_0} \tag{9}$$

The subscript 0 denotes the zero-order values, $T = t_f - t_0$, $\hat{t} - t_0 = (t - t_0)T_0/T$, and T_0 is the zero-order approximation for T.

Higher-Order Problems

All of the higher-order corrections obey the following time-varying, linear, nonhomogeneous equations:

$$\frac{\mathrm{d}}{\mathrm{d}\hat{t}}\begin{bmatrix} x_k \\ \lambda_k \end{bmatrix} = \begin{bmatrix} A_{11}(x_0, \lambda_0, T_0) & A_{12}(x_0, \lambda_0, T_0) \\ A_{21}(x_0, \lambda_0, T_0) & A_{22}(x_0, \lambda_0, T_0) \end{bmatrix}\begin{bmatrix} x_k \\ \lambda_k \end{bmatrix}$$

$$+ \frac{T_k}{T_0}\begin{bmatrix} C_1(x_0, \lambda_0, T_0) \\ C_2(x_0, \lambda_0, T_0) \end{bmatrix}$$

$$+ \begin{bmatrix} P_{1k}(x_0, \lambda_0, T_0, \ldots, x_{k-1}, \lambda_{k-1}, T_{k-1}) \\ P_{2k}(x_0, \lambda_0, T_0, \ldots, x_{k-1}, \lambda_{k-1}, T_{k-1}) \end{bmatrix}$$

$$\hat{t} \in [t_0, t_0 + T_0] \tag{10}$$

for appropriate boundary and transversality conditions obtained by expansion of the boundary and transversality conditions of the original problem, where k denotes the order of the correction. The various A, C, and P in Eq. (10) are defined in Eqs. (14) and (15) of Ref. 12. Note that the various A and C depend only on the zero-order solution and that $\hat{t} \varepsilon [t_0, t_0 + T_0]$ so that the higher-order solution terms are defined over the same time interval as the zero-order solution. The solution can be expressed as

$$\begin{bmatrix} x_k(\hat{t}) \\ \lambda_k(\hat{t}) \end{bmatrix} = \Omega_A(\hat{t}, t_0)\begin{bmatrix} x_k(t_0) \\ \lambda_k(t_0) \end{bmatrix} + \frac{T_k}{T_0}\int_{t_0}^{\hat{t}} \Omega_A(\hat{t}, \tau)\begin{bmatrix} C_1 \\ C_2 \end{bmatrix} \mathrm{d}\tau$$

$$+ \int_{t_0}^{\hat{t}} \Omega_A(\hat{t}, \tau)\begin{bmatrix} P_{1k} \\ P_{2k} \end{bmatrix} \mathrm{d}\tau \tag{11}$$

where Ω_A is the state transition matrix for the linear system in Eq. (10). Using the previous expression at $\hat{t} = t_0 + T_0$ along with the expansions of the boundary and transversality conditions, the solution for $\lambda_k(t_0)$, ν_k, and T_k is obtained from a set of linear algebraic equations. The major part of the computation for the higher-order terms lies in the quadrature that must be performed in Eq. (11).

After forming the series expansion for $x(\hat{t})$ and $\lambda(\hat{t})$ to any order, an open-loop approximation for $x(t)$ and $\lambda(t)$ may be constructed by using the definition for $\hat{t}$ with T obtained from its series expansion (using the computed values of T_k). This in effect stretches (or shrinks) the response (as viewed on the $\hat{t}$ time scale) so that it varies over the interval $t \varepsilon [t_0, T]$.

Implementation for Closed-Loop Guidance

If the solution process is terminated at, say, $k = 1$, then a real-time sampled data implementation of the control solution would be constructed as follows. For the original system in Eq. (2), an expression for the optimal control is obtained as a function of x and λ from the optimality condition in Eq. (4). Then, treating the present state as the initial state, a first-order approximation is obtained by using $\lambda_0(t_0) + \varepsilon\lambda_1(t_0)$ as an approximation for $\lambda(t_0)$ to compute the control, where $\lambda_0(t_0)$ and $\lambda_1(t_0)$ are obtained from the solutions of the zero necessary conditions and Eq. (10) for $k = 1$. This process is repeated at the next control update time by regarding the value of the state as the new initial state.

If the current state is regarded as the initial state, then $x_k(t_0) = 0$ in Eq. (11) since $x_0(t_0)$ satisfies the initial condition on the state variable. Since the zero-order solution changes at each update of the initial state, it is necessary to repeat the quadrature at each update for the higher-order corrections. Alternatively, we can fix the zero-order solution and treat $x_1(t_0)$ as the deviation between the current state and the zero-order solution computed for the original epoch time but evaluated at the present time. In this form it would also be possible to precompute the quadrature and store it as a function of a monotonic variable along the trajectory. Thus the real-time process of solving the zero-order problem and the quadrature can be avoided.

Method of Collocation

Collocation is a method for constructing an approximate solution to a set of differential equations by segmenting the time interval and representing the solution by piecewise polynomials or other simple analytic interpolating functions. The unknown coefficients of the interpolating functions within each segment are determined by enforcing continuity at the nodes, and the time derivatives of the interpolating functions satisfy the differential equations at specified points within each segment. In this section we consider an optimization problem with unperturbed dynamics $\mathrm{d}x/\mathrm{d}t = f(x, u, t)$ and Hamiltonian $H = \lambda^T f$. For simplicity of exposition, assume first-order polynomial interpolation, where the derivative constraints are enforced at the midpoint of each segment. These constraints can be expressed as

$$p_j = \frac{x_j - x_{j-1}}{\hat{t}_j - \hat{t}_{j-1}} = \left.\frac{\partial H}{\partial \lambda}\right|_{\hat{t}=(\hat{t}_j+\hat{t}_{j-1})/2;x=(x_j+x_{j-1})/2;\lambda=(\lambda_j+\lambda_{j-1})/2} \tag{12}$$

$$q_j = \frac{\lambda_j - \lambda_{j-1}}{\hat{t}_j - \hat{t}_{j-1}} = -\left.\frac{\partial H}{\partial x}\right|_{\hat{t}=(\hat{t}_j+\hat{t}_{j-1})/2;x=(x_j+x_{j-1})/2;\lambda=(\lambda_j+\lambda_{j-1})/2} \tag{13}$$

$$x(\hat{t}) = x_{j-1} + p_j(\hat{t} - \hat{t}_{j-1}); \qquad j = 1, \ldots, N \tag{14}$$

$$\lambda(\hat{t}) = \lambda_{j-1} + q_j(\hat{t} - \hat{t}_{j-1}); \qquad \hat{t} \in [\hat{t}_{j-1}, t_j]$$
$$\hat{t}_0 = t_0; \qquad \hat{t}_N = t_0 + T_0 \tag{15}$$

where N is the number of segments. The control is assumed to have been eliminated using the optimality condition in Eq. (4).

A regular perturbation formulation may be introduced by rewriting the actual dynamics in the following form:

$$\dot{x} = p_j + \varepsilon(H_\lambda - p_j) \tag{16}$$

$$\dot{\lambda} = q_j + \varepsilon(-H_x - q_j) \tag{17}$$

$$H_u = 0; \qquad \hat{t} \in [\hat{t}_{j-1}, \hat{t}_j] \tag{18}$$

Note that ε has been artificially introduced as a bookkeeping parameter for the perturbation analysis and has a nominal value of 1.0. The justification for this step is that if the collocation solution alone accurately approximates the true solution, then the second terms in Eqs. (16) and (17) may be regarded as having a small perturbing effect on the state and costate derivatives, which is actually zero at the midpoints of the segments. Once the control is eliminated using Eq. (18), then we have a two-point boundary-value problem defined by Eqs. (16) and (17), whose solution we seek by regular expansion. The zero-order solution is obtained numerically by collocation with linear interpolation in each segment. The higher-order corrections when performed provide an improvement to the collocation solution without increasing the number of nodes, thus providing a hybrid approach.

If the control cannot be eliminated explicitly by using Eq. (18), then an analytic portion $\Pi(u, x, \lambda)$ of the optimality condition (for which it is possible to eliminate u) can be extracted, by expressing the optimality condition as

$$0 = \Pi + \varepsilon(H_u - \Pi) \tag{19}$$

Then, in the zero-order problem, $\Pi = 0$ is used to eliminate the control. This approach was used in the launch vehicle application treated in the following section. The various A, C, and P of the linear differential equations for first- and higher-order corrections of the collocation solution, which correspond to Eq. (10), are given in Eqs. (24) and (25) of Ref. 12.

In practice it is advantageous to select interpolating functions that are more complex than the simple first-order forms in Eqs. (12–15). In the next section we incorporate the approach in Ref. 12 of utilizing the analytically tractable portion of the necessary conditions to define the interpolating functions for a launch vehicle guidance problem. This amounts to employing a bilinear tangent law, whose linear version is optimal under the assumptions of a flat, nonrotating Earth and zero atmospheric forces.[9]

Launch Vehicle Ascent Trajectory Guidance

The guidance problem is to find the thrust-vector angle program for maximizing payload. For illustrative purposes we assume a two-stage rocket vehicle with specified staging time t_s and a specified stage mass m_s after first-stage jettison. The trajectory is assumed to have no coasting flight.

Using a point mass model about a nonrotating spherical Earth in a nonstationary atmosphere, the equations of planar motion in the rectangular coordinates shown in Fig. 1 are

$$\dot{m} = -T_{\text{vac}}^{(i)}/[g_e I_{\text{sp}}^{(i)}] = -k^{(i)}; \qquad m(t_0) = m_0$$
$$m(t_{s+}) = m_s$$
$$\dot{v} = [T^{(i)} \sin\theta - D^{(i)} \sin\gamma + L^{(i)} \cos\gamma]/m - \mu_e/r^2 + u^2/r$$
$$v(t_0) = v_0$$
$$\dot{u} = [T^{(i)} \cos\theta - D^{(i)} \cos\gamma - L^{(i)} \sin\gamma]/m - uv/r$$
$$u(t_0) = u_0$$
$$\dot{r} = v; \qquad r(t_0) = r_0$$
$$\dot{\phi} = u/r; \qquad \phi(t_0) = \phi_0 \tag{20}$$

where

$$g_e = \mu_e/r^2$$
$$L^{(i)} = qS^{(i)}C_L^{(i)}(M, \alpha); \qquad D^{(i)} = qS^{(i)}C_D^{(i)}(M, \alpha)$$
$$T^{(i)} = T_{\text{vac}}^{(i)} - pA_e^{(i)}$$
$$q = \rho V^2/2; \qquad V = \sqrt{(v - w_r)^2 + (u - w_\phi)^2}$$
$$M = V/c$$
$$\alpha = \theta - \gamma; \qquad \gamma = \tan^{-1}[(v - w_r)/(u - w_\phi)] \tag{21}$$

In Eqs. (21), w_r and w_ϕ are the wind velocity components, V is the total airspeed, and c is the speed of sound. The superscript (i) indicates different stage values. The state variables v and u are the local vertical and horizontal velocity components, respectively, r is magnitude of the radial vector measured from the center of the Earth ($r_e = 6.378 \times 10^6$ m), ϕ is the downrange angle, and m is the vehicle mass. The control variable is θ, the thrust-vector angle measured from the local horizon. The Earth's gravitational constant is $\mu_e(3.9906 \times 10^{14}\ \text{m}^3\text{s}^{-2})$, k is the stagewise constant fuel mass rate, T_{vac} is the vacuum thrust, $p(\rho)$ is the atmospheric pressure (density), and A_e is the engine nozzle exit area. The wind has components of w_r and w_ϕ in the local vertical and horizontal directions. The remaining variables are standard notation as used in flight mechanics. The aerodynamic coefficients are in general functions of Mach number and angle of attack. The atmospheric model for p, ρ, and c is based on the 1975 U.S. Standard Atmosphere.[13] Spline fits

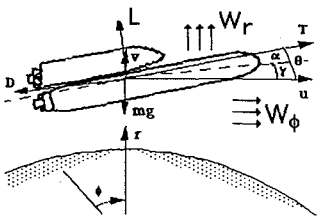

Fig. 1 Launch vehicle rectangular coordinate system.

are used to interpolate the aerodynamic coefficients and the standard atmospheric properties.

Before proceeding, we will simplify the problem formulation. Since the dynamics and performance index are independent of ϕ, and the final downrange angle is open, its dynamics can be treated separately. Also we will eliminate the mass state using

$$m(t) = \begin{cases} m_0 - k^{(1)}(t - t_0); & t_0 \le t \le t_S \\ m_S - k^{(2)}(t - t_S); & t_S \le t \le t_f \end{cases} \tag{22}$$

The equivalent performance objective is to maximize $-t_f$.

Hybrid Formulation

As discussed earlier, it is possible to improve a collocation solution by using more intelligent interpolating functions than the first-order representations in Eqs. (14) and (15). The interpolating functions can be derived from analysis of the analytically tractable portions in the necessary conditions. In this case if spherical Earth and atmospheric effects are neglected, then a linear tangent law guidance solution results.[8,9] However, the costate dynamics are poorly represented as either constant or zero. Hence, the strategy is to retain the state dynamics approximation and use the collocation method to improve the representation of the costates (cf. level 2 formulation in Ref. 12). This also reduces the number of unknowns by half. Thus, instead of using Eqs. (12) and (13) to interpolate both the states and costates, only the latter were chosen. The perturbed collocation formulation in Eqs. (16) and (17) becomes

$$\dot{v} = \frac{T_{\text{vac}}^{(i)} - \bar{p}^{(i)}A_e^{(i)}}{m(t)} \sin\theta - \bar{g}_v^{(i)} + \varepsilon\left\{\frac{[\bar{p}^{(i)} - p]A_e^{(i)} \sin\theta - D^{(i)} \sin\gamma + L^{(i)} \cos\gamma}{m(t)} + \bar{g}_v^{(i)} - \frac{\mu_e}{r^2} + \frac{u^2}{r}\right\}$$
$$\dot{u} = \frac{T_{\text{vac}}^{(i)} - \bar{p}^{(i)}A_e^{(i)}}{m(t)} \cos\theta - \bar{g}_u^{(i)} + \varepsilon\left\{\frac{[\bar{p}^{(i)} - p]A_e^{(i)} \cos\theta - D^{(i)} \cos\gamma + L^{(i)} \sin\gamma}{m(t)} + \bar{g}_u^{(i)} - \frac{uv}{r}\right\} \tag{23}$$
$$\dot{r} = v$$
$$\dot{\lambda}_v = q_{vj} + \varepsilon\left(-\frac{\partial H}{\partial v} - q_{vj}\right); \qquad j = 1, \ldots, N$$
$$\dot{\lambda}_u = q_{uj} + \varepsilon\left(-\frac{\partial H}{\partial u} - q_{uj}\right)$$
$$\dot{\lambda}_r = q_{rj} + \varepsilon\left(-\frac{\partial H}{\partial r} - q_{rj}\right)$$
$$\frac{\partial}{\partial\theta}(\lambda_v \dot{v} + \lambda_u \dot{u} + \lambda_r \dot{r}) = 0$$

where

$$H = \lambda_v \left\{ \frac{[T_{\text{vac}}^{(i)} - pA_e^{(i)}]\sin\theta - D^{(i)}\sin\gamma + L^{(i)}\cos\gamma}{m(t)} - \frac{\mu_e}{r^2} + \frac{u^2}{r} \right\} + \lambda_u \left\{ \frac{[T_{\text{vac}}^{(i)} - pA_e^{(i)}]\cos\theta - D^{(i)}\cos\gamma - L^{(i)}\sin\gamma}{m(t)} - \frac{uv}{r} \right\} + \lambda_r v; \qquad H(t_f) = 1 \tag{24}$$

The terms $\bar{p}^{(i)}$, $\bar{g}_v^{(i)}$, and $\bar{g}_u^{(i)}$ are approximations for the average values of the nozzle back pressure and the spherical acceleration components for each flight stage.

In the following we make use of the analytic portion of the optimality condition in Eq. (23) to generate the zero-order control. This is done by using the form in Eq. (19), with Π defined by excluding the aerodynamic and back pressure component of thrust in H. This amounts to regarding the dependence of aerodynamic forces on θ as a perturbation of the optimality condition, which results in the familiar bilinear tangent law

$$\tan\theta_0(t) = \frac{\lambda_{v0j-1} + q_{vj}(t - t_{j-1})}{\lambda_{u0j-1} + q_{uj}(t - t_{j-1})} \tag{25}$$

Zero-Order Solution

With the previous formulation and using the expression in Eq. (25) to eliminate the control, the zero-order solution ($\varepsilon = 0$) can be expressed as

$$v_0(t) = v_0(t_{j-1}) + \frac{FD}{k^{(i)}} \times \left\{ \frac{\zeta + \Delta}{\sqrt{1+\Delta^2}} \sinh^{-1}[\tan(\varphi + \eta)] - \sinh^{-1}(\tan\varphi) \right\} \Bigg|_{\varphi(t_{j-1})}^{\varphi(t)} - (t - t_{j-1})\bar{g}_v^{(i)}; \quad t \in [t_{j-1}, t_j]$$

$$u_0(t) = u_0(t_{j-1}) + \frac{FE}{k^{(i)}} \times \left\{ \frac{1 + \Delta\xi}{\sqrt{1+\Delta^2}} \sinh^{-1}[\tan(\varphi + \eta)] - \xi \sinh^{-1}(\tan\varphi) \right\} \Bigg|_{\varphi(t_{j-1})}^{\varphi(t)} - (t - t_{j-1})\bar{g}_u^{(i)} \tag{26}$$

$$r_0(t) = r_0(t_{j-1}) - \frac{FDC}{k^{(i)}A} \times \left((\Delta - \tan\varphi) \left\{ \frac{\zeta + \Delta}{\sqrt{1+\Delta^2}} \sinh^{-1}[\tan(\varphi + \eta)] - \sinh^{-1}(\tan\varphi) \right\} - \sec\varphi - \zeta \sinh^{-1}(\tan\varphi) \right) \Bigg|_{\varphi(t_{j-1})}^{\varphi(t)} + \left[v_0(t_{j-1}) - \bar{g}_v^{(i)} \frac{t - t_{j-1}}{2} \right](t - t_{j-1}) - G(t_{j-1})$$

$$\lambda_{v0}(t) = \lambda_{v0j-1} + q_{vj}(t - t_{j-1})$$
$$\lambda_{u0}(t) = \lambda_{u0j-1} + q_{uj}(t - t_{j-1})$$
$$\lambda_{r0}(t) = \lambda_{r0j-1} + q_{rj}(t - t_{j-1})$$

where

$$A = \sqrt{q_{vj}^2 + q_{uj}^2}; \qquad B = (c_v q_{vj} + c_u q_{uj})/A$$
$$C = \sqrt{c_v^2 + c_u^2 - B^2}; \qquad D = q_{vj}/A$$
$$E = (c_u A - q_{uj}B)/(AC); \qquad F = T_{\text{vac}}^{(i)} - \bar{p}^{(i)}A_e^{(i)}$$
$$c_v = \lambda_{v0j-1} - q_{vj}t_{j-1}; \qquad c_u = \lambda_{u0j-1} - q_{uj}t_{j-1}$$
$$c_m = m^{(i)} + k^{(i)}t_{j-1}; \qquad \xi = q_{uj}/(EA)$$
$$\Delta = [c_m A + k^{(i)}B]/k^{(i)}/C; \qquad \zeta = (c_v A - q_{vj}B)/(q_{vj}C)$$
$$\varphi(t) = \tan^{-1}\left(\frac{At + B}{C}\right); \qquad \eta = \begin{cases} \tan^{-1}(1/\Delta), & \Delta \geq 0 \\ \pi + \tan^{-1}(1/\Delta), & \Delta < 0 \end{cases}$$

$$G(t_{j-1}) = \frac{FD}{k^{(i)}} \left\{ \frac{\zeta + \Delta}{\sqrt{1+\Delta^2}} \sinh^{-1}[\tan(\varphi + \eta)] - \sinh^{-1}(\tan\varphi) \right\} \Bigg|_{\varphi(t_{j-1})} \tag{27}$$

The previous expressions constitute a set of nonlinear interpolating functions, and the zero-order solution is now expressed in terms of the unknown nodal values for the costates. To evaluate these nodal values, the collocation constraints in Eq. (13) are employed:

$$q_{vj} = \frac{\lambda_{v0j} - \lambda_{v0j-1}}{t_j - t_{j-1}} = -\frac{\partial H}{\partial v}\Bigg|_{\substack{t=(t_j+t_{j-1})/2;\lambda_{v0}=(\lambda_{v0j}+\lambda_{v0j-1})/2;\\ \lambda_{u0}=(\lambda_{u0j}+\lambda_{u0j-1})/2;\lambda_{r0}=(\lambda_{r0j}+\lambda_{r0j-1})/2}} \tag{28}$$

$$q_{uj} = \frac{\lambda_{u0j} - \lambda_{u0j-1}}{t_j - t_{j-1}} = -\frac{\partial H}{\partial u}\Bigg|_{t=(t_j+t_{j-1})/2;\ldots;\lambda_{r0}=(\lambda_{r0j}+\lambda_{r0j-1})/2} \tag{29}$$

$$q_{rj} = \frac{\lambda_{r0j} - \lambda_{r0j-1}}{t_j - t_{j-1}} = -\frac{\partial H}{\partial r}\Bigg|_{t=(t_j+t_{j-1})/2;\ldots;\lambda_{r0}=(\lambda_{r0j}+\lambda_{r0j-1})/2} \tag{30}$$

Since more control activity is expected in the atmospheric phase of flight, a denser segmentation is recommended for the first-stage flight, whereas a one-piece segment is sufficient for the subsequent more nearly exoatmospheric second-stage flight.

First-Order Solution

The linear differential equation satisfied by the first-order terms has the following form:

$$\frac{d}{dt}\begin{bmatrix} v_1 \\ u_1 \\ r_1 \\ \lambda_{v1} \\ \lambda_{u1} \\ \lambda_{r1} \end{bmatrix} = \begin{bmatrix} 0 & 0 & 0 & a_{14j} & a_{15j} & 0 \\ 0 & 0 & 0 & a_{15j} & a_{25j} & 0 \\ 1 & 0 & 0 & 0 & 0 & 0 \\ \frac{\partial q_{vj}}{\partial v} & \frac{\partial q_{vj}}{\partial u} & \frac{\partial q_{vj}}{\partial r} & \frac{\partial q_{vj}}{\partial \lambda_v} + f_1\frac{\partial q_{vj}}{\partial \theta} & \frac{\partial q_{vj}}{\partial \lambda_u} + f_2\frac{\partial q_{vj}}{\partial \theta} & -1 \\ \frac{\partial q_{uj}}{\partial v} & \frac{\partial q_{uj}}{\partial u} & \frac{\partial q_{uj}}{\partial r} & \frac{\partial q_{uj}}{\partial \lambda_v} + f_1\frac{\partial q_{uj}}{\partial \theta} & \frac{\partial q_{uj}}{\partial \lambda_u} + f_2\frac{\partial q_{uj}}{\partial \theta} & 0 \\ \frac{\partial q_{rj}}{\partial v} & \frac{\partial q_{rj}}{\partial u} & \frac{\partial q_{rj}}{\partial r} & \frac{\partial q_{rj}}{\partial \lambda_v} + f_1\frac{\partial q_{rj}}{\partial \theta} & \frac{\partial q_{rj}}{\partial \lambda_u} + f_2\frac{\partial q_{rj}}{\partial \theta} & 0 \end{bmatrix} \times \begin{bmatrix} v_1 \\ u_1 \\ r_1 \\ \lambda_{v1} \\ \lambda_{u1} \\ \lambda_{r1} \end{bmatrix} + \frac{T_1}{T_0}\begin{bmatrix} c_{1j}(t) \\ c_{2j}(t) \\ v_0(t) \\ q_{vj} \\ q_{uj} \\ q_{rj} \end{bmatrix} + \begin{bmatrix} p_{1j}(t) \\ p_{2j}(t) \\ 0 \\ p_{4j}(t) \\ p_{5j}(t) \\ p_{6j}(t) \end{bmatrix}; \quad t \in [t_{j-1}, t_j] \tag{31}$$

Complete expressions are given in the Appendix. Since the first-stage flight time is assumed to be fixed, $T_1 = 0$ for the dynamics describing $t \le t_s$, and the second term in Eq. (31) is discarded for the segments corresponding to this time interval.

Experience has shown that higher-order perturbation corrections are not sensitive to using an exact state transition matrix. This behavior is analogous to the practice of using an approximate Jacobian to solve nonlinear algebraic equations. Therefore, we introduced the following approximation to simplify the analysis. The 3×5 lower left corner block of the system matrix in Eq. (31) represents the effects that second-order variations of the atmospheric terms have on the costate variables. By neglecting these terms we are able to derive an approximate state transition matrix for the first-order system:

$$\Omega^{(i)}_{A_j}(t, t_{j-1}) = \begin{bmatrix} 1 & 0 & 0 & \omega^{(i)}_{14_j} & \omega^{(i)}_{15_j} & \omega^{(i)}_{16_j} \\ 0 & 1 & 0 & \omega^{(i)}_{24_j} & \omega^{(i)}_{25_j} & \omega^{(i)}_{26_j} \\ t - t_{j-1} & 0 & 1 & \omega^{(i)}_{34_j} & \omega^{(i)}_{35_j} & \omega^{(i)}_{36_j} \\ 0 & 0 & 0 & 1 & 0 & t_{j-1} - t \\ 0 & 0 & 0 & 0 & 1 & 0 \\ 0 & 0 & 0 & 0 & 0 & 1 \end{bmatrix}; \quad t \in [t_{j-1}, t_j] \tag{32}$$

The Appendix details the ω terms in Eq. (32). The lower right-hand block in Eq. (32) accounts for spherical Earth effects on the costate solution, neglected in the zero-order solution. As will be shown in the numerical results section, this is an important correction for the exoatmospheric phase of flight.

By successively applying Eq. (11) N times, the first-order perturbations at t_N (the zero-order final time) are given by

$$\begin{bmatrix} x_1(t_N) \\ \lambda_1(t_N) \end{bmatrix} = \Omega^{(2)}_{A_N}(t_N, t_{N-1})\Omega^{(1)}_{A_{N-1}}(t_{N-1}, t_{N-2}) \cdots \Omega^{(1)}_{A_1}(t_1, t_0) \times \begin{bmatrix} x_1(t_0) \\ \lambda_1(t_0) \end{bmatrix} + \int_{t_{N-1}}^{t_N} \Omega^{(2)}_{A_N}(t_N, \tau) \left\{ \frac{T_1}{T_0} \begin{bmatrix} C^{(2)}_{1_N}(\tau) \\ C^{(2)}_{2_N}(\tau) \end{bmatrix} + \begin{bmatrix} P^{(2)}_{1_N}(\tau) \\ P^{(2)}_{2_N}(\tau) \end{bmatrix} \right\} d\tau + \sum_{j=1}^{j=N-1} \Omega^{(2)}_{A_N}(t_N, t_{N-1}) \cdots \Omega^{(1)}_{A_{j+1}}(t_{j+1}, t_j) \times \int_{t_{j-1}}^{t_j} \Omega^{(1)}_{A_j}(t_j, \tau) \begin{bmatrix} P^{(1)}_{1_j}(\tau) \\ P^{(1)}_{2_j}(\tau) \end{bmatrix} d\tau \tag{33}$$

Advanced Launch System Application

This application considers a generic model for an advanced launch system (ALS). It has an asymmetric configuration, with the booster mounted atop the main body as illustrated in Fig. 1. The aerodynamic coefficients were taken from Ref. 14 and interpolated with bicubic splines as functions of Mach number and angle of attack. Because of the asymmetric configuration, a shadowing effect is created by the booster above the sonic speed. This results in a nonconvex dependence of C_D on angle of attack, as illustrated in Fig. 2.

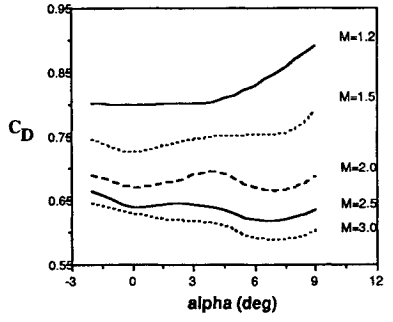

Fig. 2 ALS first-state C_D profile.

The boundary conditions on the state variables simulate a vertical launch to direct injection at the perigee of an 80 × 150 n.mi, elliptical transfer orbit: $t_0 = 15$ s, $v_0 = 64.49$ ms^{-1}, $u_0 = 0.56$ ms^{-1}, $h_0 = 400$ m, $v_f = 0$, $u_f = 7858.2$ ms^{-1}, and $h_f = 148,160$ m. The physical parameters of the vehicle are given in Table 1. The staging time t_s is 158.5 s. Other parameters chosen for this problem are

$$\bar{p}^{(1)} = p(h_0)/2; \qquad \bar{g}^{(1)}_v = \mu_e/r_0^2 - u_0^2/r_0; \qquad \bar{g}^{(1)}_u = 0$$
$$\bar{p}^{(2)} = 0; \qquad \bar{g}^{(2)}_v = \bar{g}^{(1)}_v/2; \qquad \bar{g}^{(2)}_u = 0 \tag{34}$$

These parameters are updated when generating the feedback control that is done at every second. The terminal boundary and transversality conditions in this case are

$$v(t_f) = v_f; \qquad u(t_f) = u_f$$
$$h(t_f) = h_f; \qquad (\lambda_v \dot{v} + \lambda_u \dot{u} + \lambda_r \dot{r})|_{t_f} = 1 \tag{35}$$

The total number of unknowns to be solved in the zero-order problem is $3N + 4$. These are q_{vj}, q_{uj}, and q_{rj} for $j = 1, \ldots, N$, the final time t_N, and the costate values at the final time. Open-loop solutions in a stationary atmosphere for several increasing values of N are given in Figs. 3–6. The segmentation is $N-1$ segments for the first-stage flight and one segment for the second-stage flight. Zero-order results use only the regular perturbation approach as given in Ref. 8. Significant improvements are observed in the costate profiles (Figs. 4–6) with the hybrid approach since the aerodynamic effects are partially accounted for in the zero-order formulation. This is due to the midpoint constraints in Eqs. (28–30). In particular, note from Figs. 4–6 that the zero-order solution of Ref. 8 (which amounts to ignoring aerodynamic effects and invoking a flat, nonrotating Earth approximation) results in λ_u and λ_r being constant and λ_v being linear in time, which from Eq. (25) gives the well-known linear tangent

Table 1 ALS vehicle physical data

	First stage	Second stage
m_0; m_s, kg	1,523,400	546,600
T_{vac}, N	25,813,000	7,744,000
I_{sp}, s	430	430
S, m^2	131.34	65.67
A_e, m^2	37.51	11.25

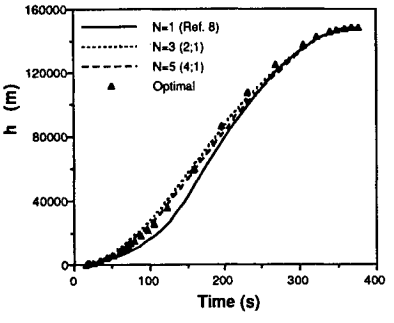

Fig. 3 Open-loop altitude profiles.

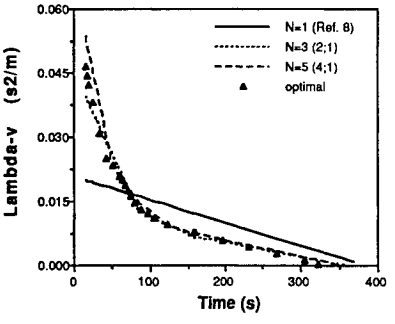

Fig. 4 Open-loop vertical velocity costate profiles.

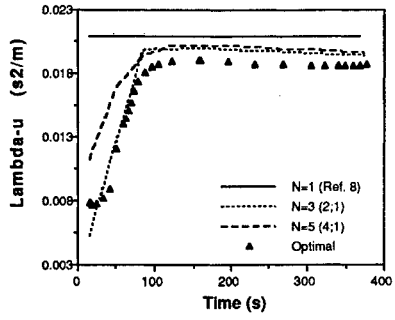

Fig. 5 Open-loop horizontal velocity costate profiles.

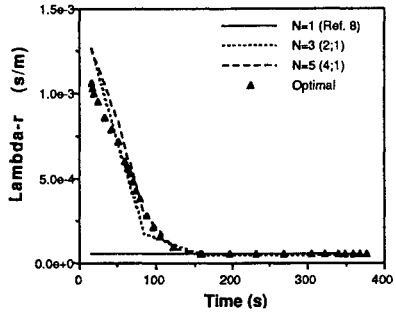

Fig. 6 Open-loop altitude costate profiles.

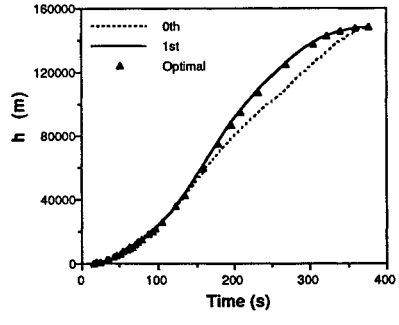

Fig. 7 Closed-loop altitude profiles.

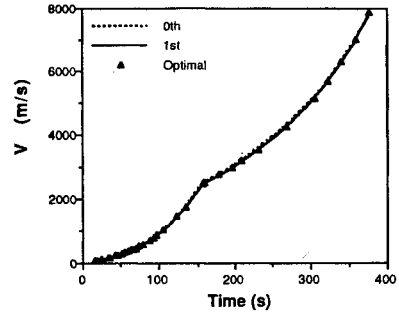

Fig. 8 Closed-loop airspeed profiles.

steering law. This largely accounts for the failure of the regular perturbation method when aerodynamic effects are included.[10]

Figures 7–11 show the closed-loop results for the state variables expressed in wind frame coordinates. The total number of segments used in this case is $N = 8$. Note in Fig. 10 that jumps in angle of attack occur at about $M = 1.3$ ($t = 64$ s) and $M = 2.3$ ($t = 91$s). These are due to the nonconvex C_D profile that gives rise to nonconvexity in the Hamiltonian. In this case it is possible to rule out the possibility of a chattering arc.[17] There is another third small jump at the staging time due to the discontinuous dynamics. Figure 10 also shows a major difference between the zero- and first-order solution for α during the end of the second-stage flight, which is due to the absence of the spherical Earth corrections in the zero-order solution. Even though a large difference exists between the two solutions, the trajectory and the performance index stay very close and imply that

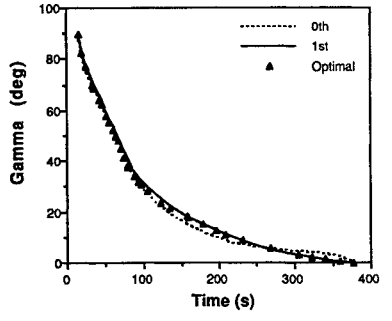

Fig. 9 Closed-loop flight-path angle profiles.

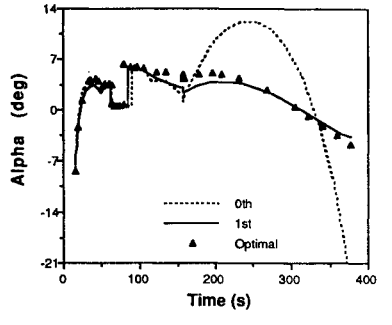

Fig. 10 Closed-loop angle of attack profiles.

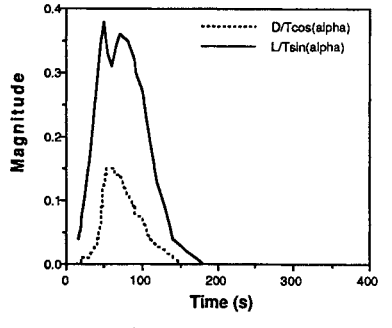

Fig. 11 Aerodynamic to propulsive force ratios.

the optimal result is not sensitive to control variations. However, the example reveals that the aerodynamic forces have a significant effect in the middle portion of the first-stage ascent. This is illustrated in Fig. 11, which shows the ratios of the lift and drag forces to the corresponding thrust components. This explains why the regular perturbation analysis in Ref. 8 was not able to correct for the effect of aerodynamic forces in the first-order analysis. These forces are simply too large to be treated as perturbations, and consequently the calculated first-order correction diverged.[10] Use of the collocation method in forming a zero-order solution largely accounts for the aerodynamic effect through the midsegment constraints in Eqs. (28–30).

Remarks on the Numerical Results

The results show a high level of fidelity and justify the approximation we introduced to obtain the state transition matrix in Eq. (32). In particular, the first-order solution shows significant improvement by correcting for spherical Earth effects, as illustrated in Fig. 10. In this case the zero-order solution failed to anticipate the sharp change in the radial acceleration as the orbital condition is approached, even using a continuously updated guess of $\bar{g}_v$. This results in an excessive pull-up of the vehicle during the initial portion of the second-stage flight, which is later corrected by a large negative α profile to meet the terminal conditions. However, both zero- and first-order results give extremely good orbit injection accuracy without requiring a high rate of control update.

The computations for the cases presented here were done on a SPARCstation 1. The maximum CPU time needed for a control update was 0.65 s for the eight-segment solution. The Newton method with Broyden's update of the Jacobian[15] used in the zero-

order collocation evaluation converged typically in four iterations. Computation time could likely be further enhanced by using sparse Broyden update techniques.[16] It is apparent from the numerical results that the first-order correction is needed mainly to correct for spherical Earth effects that are dominant only in the second stage of flight. Therefore a significant additional savings in computation time would have resulted had we computed this correction only for that phase.

Conclusions

A hybrid approach to launch vehicle ascent guidance using a combined analytic/numerical approach employing perturbation and collocation techniques has been demonstrated for a significant application. The feedback approach is to first solve the zero-order costate approximates formulated by a collocation method and then obtain first-order corrections by regular perturbation analysis. By employing intelligent interpolating functions that are derived from the necessary conditions, the collocation solution can be obtained using a small number of segments. Thus, many of the shortcomings of purely analytical and purely numerical approaches are diminished, which has important implications for real-time guidance. For launch vehicle guidance, the approach extends the bilinear tangent law so that it can be used for both atmospheric and exoatmospheric flight phases, including final precision orbit injection. The resulting solution may be interpreted as one in which the parameters of the steering law are adjusted for each segment of the trajectory as the vehicle passes through the atmosphere.

Appendix

The following are the expressions for Eq. (31):

$$a_{14j} = \frac{T_{\text{vac}}^{(i)} - \bar{p}A_e^{(i)}}{m(t)}\left[\frac{\lambda_{u0}^2}{(\lambda_{v0}^2+\lambda_{u0}^2)^{3/2}}\right]$$

$$a_{15j} = \frac{T_{\text{vac}}^{(i)} - \bar{p}A_e^{(i)}}{m(t)}\left[\frac{-\lambda_{v0}\lambda_{u0}}{(\lambda_{v0}^2+\lambda_{u0}^2)^{3/2}}\right]$$

$$a_{25j} = \frac{T_{\text{vac}}^{(i)} - \bar{p}A_e^{(i)}}{m(t)}\left[\frac{\lambda_{v0}^2}{(\lambda_{v0}^2+\lambda_{u0}^2)^{3/2}}\right]$$

$$f_1 = \frac{-\cos\theta_0}{\lambda_{v0}\sin\theta_0 + \lambda_{u0}\cos\theta_0}$$

$$f_2 = \frac{\sin\theta_0}{\lambda_{v0}\sin\theta_0 + \lambda_{u0}\cos\theta_0} \tag{A1}$$

$$c_{1j} = \frac{T_{\text{vac}}^{(i)} - \bar{p}A_e^{(i)}}{m(t)}\left[1 + \frac{(t-t_{j-1})k^{(i)}}{m(t)}\right]\frac{\lambda_{v0}}{\sqrt{\lambda_{v0}^2+\lambda_{u0}^2}} - \bar{g}_v$$

$$c_{2j} = \frac{T_{\text{vac}}^{(i)} - \bar{p}A_e^{(i)}}{m(t)}\left[1 + \frac{(t-t_{j-1})k^{(i)}}{m(t)}\right]\frac{\lambda_{u0}}{\sqrt{\lambda_{v0}^2+\lambda_{u0}^2}} - \bar{g}_u$$

$$p_{1j} = g_1 + \frac{\lambda_{u0}}{\lambda_{v0}^2+\lambda_{u0}^2}\left(\lambda_{v0}\frac{\partial g_1}{\partial\theta_0} + \lambda_{u0}\frac{\partial g_2}{\partial\theta_0}\right)$$

$$p_{2j} = g_2 - \frac{\lambda_{v0}}{\lambda_{v0}^2+\lambda_{u0}^2}\left(\lambda_{v0}\frac{\partial g_1}{\partial\theta_0} + \lambda_{u0}\frac{\partial g_2}{\partial\theta_0}\right)$$

$$p_{4j} = -\frac{\partial H}{\partial v} - q_{vj} - \frac{\partial q_{vj}}{\partial\theta}\left\{\frac{\lambda_{v0}\partial g_1/\partial\theta_0 + \lambda_{u0}\partial g_2/\partial\theta_0}{(\lambda_{v0}\sin\theta_0 + \lambda_{u0}\cos\theta_0)[T_{\text{vac}}^{(i)} - \bar{p}A_e^{(i)}]/m(t)}\right\}$$

$$p_{5j} = -\frac{\partial H}{\partial u} - q_{uj} - \frac{\partial q_{uj}}{\partial\theta}\left\{\frac{\lambda_{v0}\partial g_1/\partial\theta_0 + \lambda_{u0}\partial g_2/\partial\theta_0}{(\lambda_{v0}\sin\theta_0 + \lambda_{u0}\cos\theta_0)[T_{\text{vac}}^{(i)} - \bar{p}A_e^{(i)}]/m(t)}\right\}$$

$$p_{6j} = -\frac{\partial H}{\partial r} - q_{rj} - \frac{\partial q_{rj}}{\partial\theta}\left\{\frac{\lambda_{v0}\partial g_1/\partial\theta_0 + \lambda_{u0}\partial g_2/\partial\theta_0}{(\lambda_{v0}\sin\theta_0 + \lambda_{u0}\cos\theta_0)[T_{\text{vac}}^{(i)} - \bar{p}A_e^{(i)}]/m(t)}\right\}$$

$$\frac{\partial q_{vj}}{\partial\theta} = \left\{-\frac{\partial^2 H}{\partial\theta\partial v}\right\}\Bigg|_{t=(t_j+t_{j-1})/2;\ldots;\lambda_{r0}=(\lambda_{r0j}+\lambda_{r0j-1})/2}$$

$$\frac{\partial q_{uj}}{\partial\theta} = \left\{-\frac{\partial^2 H}{\partial\theta\partial u}\right\}\Bigg|_{t=(t_j+t_{j-1})/2;\ldots;\lambda_{r0}=(\lambda_{r0j}+\lambda_{r0j-1})/2}$$

$$\frac{\partial q_{rj}}{\partial\theta} = \left\{-\frac{\partial^2 H}{\partial\theta\partial r}\right\}\Bigg|_{t=(t_j+t_{j-1})/2;\ldots;\lambda_{r0}=(\lambda_{r0j}+\lambda_{r0j-1})/2}$$

where

$$g_1 = \frac{(p-p)A_e^{(i)}\sin\theta_0 - D^{(i)}\sin\gamma_0 + L^{(i)}\cos\gamma_0}{m(t)} + \bar{g}_v - \frac{\mu_e}{r_0} + \frac{u_0^2}{r_0} \tag{A2}$$

$$g_2 = \frac{(p-p)A_e^{(i)}\cos\theta_0 - D^{(i)}\cos\gamma_0 - L^{(i)}\sin\gamma_0}{m(t)} + \bar{g}_u - \frac{u_0 v_0}{r_0}$$

The remaining partial derivatives ($\partial q_{vj}/\partial v$, $\partial q_{vj}/\partial u$, ...) are similar to the last three expressions in Eq. (A1).

The approximate state transition matrix in Eq. (32) can be obtained by taking the partial derivatives of the analytic zero-order solution in Eq. (26) with respect to the initial conditions $[v_0(t_{j-1}), u_0(t_{j-1}), r_0(t_{j-1}), \lambda_{v0}(t_{j-1}), \lambda_{u0}(t_{j-1}), \lambda_{r0}(t_{j-1})]$. So we have

$$\omega_{14} = \frac{\partial v_0(t)}{\partial\lambda_{v0}(t_{j-1})} = \frac{\partial v_0(t)}{\partial c_v}; \qquad \omega_{15} = \frac{\partial v_0(t)}{\partial\lambda_{u0}(t_{j-1})} = \frac{\partial v_0(t)}{\partial c_u}$$

$$\omega_{16} = \frac{\partial v_0(t)}{\partial\lambda_{r0}(t_{j-1})} = -\frac{\partial v_0(t)}{\partial q_{vj}}; \qquad \omega_{24} = \frac{\partial u_0(t)}{\partial\lambda_{v0}(t_{j-1})} = \frac{\partial u_0(t)}{\partial c_v}$$

$$\omega_{25} = \frac{\partial u_0(t)}{\partial\lambda_{u0}(t_{j-1})} = \frac{\partial u_0(t)}{\partial c_u}; \qquad \omega_{26} = \frac{\partial u_0(t)}{\partial\lambda_{r0}(t_{j-1})} = -\frac{\partial u_0(t)}{\partial q_{vj}}$$

$$\omega_{34} = \frac{\partial r_0(t)}{\partial\lambda_{v0}(t_{j-1})} = \frac{\partial r_0(t)}{\partial c_v}; \qquad \omega_{35} = \frac{\partial r_0(t)}{\partial\lambda_{u0}(t_{j-1})} = \frac{\partial r_0(t)}{\partial c_u}$$

$$\omega_{36} = \frac{\partial r_0(t)}{\partial\lambda_{r0}(t_{j-1})} = -\frac{\partial r_0(t)}{\partial q_{vj}} \tag{A3}$$

For example, using the chain rule, ω_{14} is given by

$$\omega_{14} = \frac{\partial v_0}{\partial D}\frac{\partial D}{\partial c_v} + \frac{\partial v_0}{\partial\Delta}\frac{\partial\Delta}{\partial c_v} + \frac{\partial v_0}{\partial\zeta}\frac{\partial\zeta}{\partial c_v} + \frac{\partial v_0}{\partial\varphi}\frac{\partial\varphi}{\partial c_v} + \frac{\partial v_0}{\partial\eta}\frac{\partial\eta}{\partial c_v} \tag{A4}$$

Symbolic manipulation programs such as Mathematica, MACSYMA can be used to obtain the analytic expressions of the previous derivatives and to write the subroutines needed for their computation.

Acknowledgments

This research was supported by NASA Langley Research Center under Grant NAG-1-939. Daniel D. Moerder served as the contract monitor.

References

[1]Schleich, W. T., "The Space Shuttle Ascent Guidance and Control," AIAA Paper 82-1497, 1982.

[2]Rao, P. P., "Titan IIIC Preflight and Postflight Trajectory Analyses," *Journal of Guidance, Control, and Dynamics*, Vol. 7, 1984, pp. 161–166.

[3]Brusch, R. G., and Reed, T. E., "Real-Time Launch Vehicle Steering Programme Selection," *Journal of the British Interplanetary Society*, Vol. 26, 1973, pp. 279–290.

[4]Well, K. H., "Ariane V Ascent Trajectory Optimization with a First-stage Splash Down Constraint," 8th IFAC Workshop on Control Application of Nonlinear Programming and Optimization, Paris, France, 1989.

[5]Shaver, D. A., and Hull, D. G., "Advanced Launch System Trajectory Optimization Using Suboptimal Control," *Proceedings of Guidance, Navigation, and Control Conference*, 1990, pp. 892–900.

[6]Hargraves, C. R., and Paris, S. W., "Direct Trajectory Optimization Using Nonlinear Programming and Collocation," *Journal of Guidance, Control, and Dynamics*, Vol. 10, 1987, pp. 338–342.

[7]Oberle, H. J., and Grimm, W., "BNDSCO, A Program for Numerical Solution of Optimal Control Problems," English Translation of DFVLR-Mitt. 85-05, 1985.

[8]Leung, S. K., and Calise, A. J., "An Approach to Optimal Guidance of an Advanced Launch Vehicle Concept," *Proceedings of the American Control Conference*, 1990, pp. 1824–1828.

[9]Feeley, T. S., and Speyer, J. L., "A Real-Time Approximate Optimal Guidance Law for Flight in a Plane," *Proceedings of the American Control Conference*, 1990, pp. 2356–2361.

[10]Calise, A. J., Hodges, D. H., Leung, S. K., and Bless, R. R., "Optimal Guidance Law Development for an Advanced Launch System," NASA Interim Progress Rept., June–Dec. 1990.

[11]Prenter, P. M., *Splines and Variational Methods*, Wiley, New York, 1975.

[12]Calise, A. J., and Leung, M. S. K., "Hybrid Approach to the Solution of Optimal Control Problems," *Journal of Guidance, Control, and Dynamics*, Vol. 17, No. 5, 1994, pp. 966–974.

[13]Minzer, R. A., et al., "U.S. Standard Atmosphere, 1975 (COESA 1975)," Goddard Space Flight Center, NASA TR-459, 1975.

[14]Pamadi, B., and Duttion, K., "An Aerodynamic Model for the Advanced Launch System Vehicle," NASA TM, 1992 (to be published).

[15]Broyden, C. G., "A Class of Methods for Solving Nonlinear Simultaneous Equations," *Mathematics of Computation*, Vol. 19, 1965, pp. 577–583.

[16]Betts, J. T., "The Application of Sparse Broyden Updates in the Collocation Methods for Optimal Control Problems," AIAA Paper 88-4150, Aug. 1988.

[17]Calise, A. J., Hodges, D. H., Leung, S. K., and Bless, R. R., "Optimal Guidance Law Development of an Advanced Launch System," NASA Interim Progress Rept., June–Nov. 1989.